

Star Formation and Stellar Mass Assembly in Dark Matter Halos: From Giants to Dwarfs

Zhankui Lu^{1*}, H.J. Mo¹, Yu Lu², Neal Katz¹, Martin D. Weinberg¹, Frank C. van den Bosch³, Xiaohu Yang^{4,5}

¹*Department of Astronomy, University of Massachusetts, Amherst MA 01003-9305, USA*

²*Kavli Institute for Particle Astrophysics and Cosmology, Stanford, CA 94309, USA*

³*Astronomy Department, Yale University, P.O. Box 208101, New Haven, CT 06520-8101, USA*

⁴*Center for Astronomy and Astrophysics, Shanghai Jiao Tong University, n Shanghai 200240, China*

⁵*Key Laboratory for Research in Galaxies and Cosmology, Shanghai Astronomical Observatory, Nandan Road 80, Shanghai 200030, China*

ABSTRACT

The empirical model of Lu et al. (2014) is updated with recent data of galaxy stellar mass functions (SMFs). The model predicts that the slope of galaxy SMFs at $z > 2$ should be quite steep at the low mass end, beyond the current detection limit, and it is a strong prediction that can be tested against future observations. The model is used to investigate the galaxy star formation and assembly or merger histories in detail. Most of the stars in cluster centrals, corresponding to BCGs in observations, formed earlier than $z \approx 2$ but have been assembled much later. Typically, they have experienced ≈ 5 major mergers since their star formation was quenched. Milky Way mass galaxies have had on-going star formation without significant mergers since $z \approx 2$, and are thus free of significant (classic) bulges produced by major mergers. Dwarf galaxies in haloes with $M_h < 10^{11} h^{-1} M_\odot$ or $M_\star < 10^9 M_\odot$ have experienced a star formation burst at $z > 2$, followed by a nearly constant star formation rate after $z = 1$, and the stellar age decreases with stellar mass, contrary to the ‘downsizing’ trend for more massive galaxies. Major mergers are not uncommon during the early burst phase and may result in the formation of old spheroids in dwarf galaxies. We also characterise the stellar population of halo stars in different halos.

Key words: galaxies: haloes — galaxies: formation — methods: statistical

1 INTRODUCTION

Given that the hierarchical formation of dark matter haloes is the backbone of galaxy formation, and that dark matter is the dominant mass component in the Universe, understanding the origin and diversity of the galaxy population requires a solid understanding of the connection between galaxies and dark matter haloes. The last decade has seen tremendous progress in this area. By combining the galaxy-dark matter connection as a function of redshift with halo merger trees, which describe the hierarchical assembly of dark matter haloes, one obtains a statistical description of how galaxies assemble their stellar mass over time.

Such an ‘empirical’ approach is intuitive and transparent in that it describes galaxy evolution within the natural framework of hierarchical structure formation. This method was developed by Conroy et al. (2007), Conroy & Wechsler (2009) and Yang et al. (2009), and has since been applied in numerous studies (e.g. Moster et al. 2010, 2013; Behroozi et al. 2010, 2013a,b; Avila-Reese & Firmani 2011; Yang et al. 2012, 2013; Wang et al. 2013; Béthermin et al 2013). An important new insight that has resulted from this ‘empirical modelling’ approach is that there is an amazing amount of ‘regularity’ and ‘simplicity’ in galaxy demographics. In particular, the relatively mild evolution in the $M_\star - M_h$ relation with redshift is found to translate into an instantaneous star formation efficiency (i.e. the star formation rate divided by the baryon

* E-mail: lv@astro.umass.edu

accretion rate) that peaks at a characteristic halo mass of $\sim 10^{12} h^{-1} M_{\odot}$, over the entire epoch from $z = 8$ to the present day, and almost all star formation has occurred inside haloes that lie within the narrow range $10^{11} h^{-1} M_{\odot} \lesssim M_h \lesssim 10^{12} h^{-1} M_{\odot}$ (Yang et al. 2012, 2013; Leauthaud et al. 2012a,b; Behroozi et al. 2013a,b; Moster et al. 2013). In addition, these studies have shown that virtually all stellar mass is assembled *in situ*: merging is only a significant channel of mass assembly for the most massive galaxies. In what follows we will refer to this picture of galaxy formation as the ‘Slow-Evolution’ model, to emphasise that it suggests little evolution in the halo mass dependence of the star formation efficiency.

A recent study by the authors (Lu et al. 2014) has argued for an important revision to this ‘Slow-Evolution’ picture. Using data on the faint-end of the luminosity function of cluster galaxies, they show that low mass haloes ($M_h \lesssim 10^{11} h^{-1} M_{\odot}$) have to form stars efficiently, but only at high redshift ($z \gtrsim 2$). In particular, they identified $z \simeq 2$ as a new characteristic epoch in galaxy formation, where there is a fairly sudden transition in the star formation efficiency of low mass haloes. This transition leads to some interesting predictions, e.g. a significant old stellar population in present-day dwarf galaxies with $M_{\star} \leq 10^8 h^{-2} M_{\odot}$ and steep low end slopes at high redshift of the galaxy stellar mass and star formation rate functions. Interestingly, recent work based on deeper high redshift surveys provide some evidence for such a steepening.

The goal of the paper is to update the model of Lu et al. (2014) with more recent observational data and to characterise in detail the star formation and merger histories of galaxies across cosmic time with the updated model. We address questions related to *in situ* star formation versus accretion, downsizing both in star formation and assembly and mergers of galaxies and their roles in shaping galaxy morphology, and the prevalence of halo stars. Wherever possible we will contrast the differences between the ‘Slow-Evolution’ model and the modified picture advocated by Lu et al. (2014).

This paper is organised as follows. Our method to model the star formation-halo mass connection is described in §2. The overall trends in the star formation and assembly histories are described in §3. In §4, we describe the total star formation and assembly histories as a function of halo (stellar) mass, paying particular attention to *in situ* star formation versus accretion, the breakdown of downsizing, and the global star formation rate density in connection to the ionisation state of the Universe. In §5, we focus on galaxy merger rates and their implications for the morphological transformation of galaxies. In §6 we address the stellar populations of galaxies as a function of their stellar mass, paying particular attention to the properties of halo stars. Finally, we summarise our results in §7.

Throughout the paper, we use a Λ CDM cosmology with $\Omega_{m,0} = 0.273$, $\Omega_{\Lambda,0} = 0.727$, $\Omega_{b,0} = 0.0455$, $h = 0.704$, $n = 0.967$ and $\sigma_8 = 0.811$. This set of

parameters is from the seven year WMAP observations (Komatsu et al. 2011). In addition, unless stated otherwise, we adopt the stellar population synthesis model of Bruzual & Charlot (2003) and a Chabrier (2003) IMF.

2 AN EMPIRICAL MODEL OF STAR FORMATION IN DARK MATTER HALOS

2.1 The Model

In this section we provide a brief description of the model of Lu et al. (2014), which we adopt here to make model predictions, referring the reader to the original paper for details.

The hierarchical assembly of individual dark matter haloes is modelled using halo merger trees generated with the Monte-Carlo model of Parkinson et al. (2008), which is based on a modified treatment of the extended Press-Schechter formalism calibrated using N -body simulations (see Cole et al. 2008). As shown in Jiang & van den Bosch (2014), the merger trees obtained with this method are as accurate as those obtained from high-resolution N -body simulations.

We assume that the star formation rate (SFR) of a central galaxy in a halo at a given redshift z is determined by the virial mass of the host halo, $M_h(z)$, and the redshift z , and hence

$$\text{SFR} = \dot{M}_{\star} [M_h, z], \quad (1)$$

where $M_h = M_h(z)$ is the instantaneous halo mass. Lu et al. (2014) adopted the following functional form for the mass and redshift dependence:

$$\dot{M}_{\star} = \mathcal{E} \frac{f_b M_h}{\tau} (X+1)^{\alpha} \left(\frac{X+\mathcal{R}}{X+1} \right)^{\beta} \left(\frac{X}{X+\mathcal{R}} \right)^{\gamma}, \quad (2)$$

where \mathcal{E} is a free parameter that sets the overall efficiency; $f_b = \Omega_{b,0}/\Omega_{m,0}$ is the cosmic baryon mass fraction; and $\tau = (1/10 H_0) (1+z)^{-3/2}$ roughly describes the dynamical timescale of haloes at redshift z . We define the quantity X as $X \equiv M_h/M_c$ where M_c is a characteristic mass; and \mathcal{R} is a positive number smaller than 1. Hence, the SFR depends on halo mass through a piece-wise power law, with α , β , and γ being the three power indices in the three mass ranges separated by the two characteristic masses, M_c and $\mathcal{R}M_c$.

Lu et al. (2014) considered three different models. In Model I they assumed that all the model parameters were independent of redshift. However, they showed that such a model was unable to match simultaneously the observed galaxy stellar mass functions (SMFs) in the redshift range between $z = 0$ and $z = 4$. This can be remedied by allowing α to depend on redshift according to

$$\alpha = \alpha_0 (1+z)^{\alpha'}, \quad (3)$$

with both α_0 and α' being free parameters. This Model II is able to fit the SMFs from $z = 0$ to $z = 4$, and is very similar to the ‘Slow Evolution’ model discussed above; virtually all stars

form in dark matter haloes in a narrow band of halo mass: $10^{11} h^{-1} M_{\odot} \lesssim M_h \lesssim 10^{12} h^{-1} M_{\odot}$. However, this model is unable to match the steep, faint-end upturn in the cluster galaxy luminosity function at $z = 0$ (Popesso et al. 2006). This upturn requires an additional modification, namely that the parameter γ , which controls the star formation efficiency in low mass haloes, depends on redshift according to

$$\gamma = \begin{cases} \gamma_a & \text{if } z < z_c \\ (\gamma_a - \gamma_b) \left(\frac{z+1}{z_c+1} \right)^{\gamma'} + \gamma_b & \text{otherwise,} \end{cases} \quad (4)$$

so that it changes from γ_b at high- z to γ_a at low- z , with a transition redshift z_c . Performing a Bayesian inference using both the stellar mass functions from $z = 0$ to $z = 4$ and the cluster galaxy luminosity function as data constraints, Lu et al. (2014) obtained a model, Model III, that fits all the data. This model differs from the ‘Slow Evolution’ model (and thus Model II) in that it predicts efficient star formation in low mass haloes ($M_h \lesssim 10^{11} h^{-1} M_{\odot}$) but only for $z > z_c \simeq 2$. As we will see later, the value of z_c is quite well constrained. Our tests using a simpler model with $z_c = 0$, shows that the model given by equation (4) is favoured by a factor $K \approx e^{15}$ in terms of the Bayes ratio [see equation (13) in Lu et al. (2014) for the definition], demonstrating clearly that the data prefer a non-zero z_c . More complicated models are not preferred by the data.

The above SFR model is only valid for central galaxies, i.e., galaxies that reside at the centres of their dark matter host haloes, where they act as the recipients of any new gas that loses its binding energy. Motivated by the notion that galaxies quench their star formation once they become satellite galaxies (e.g., Balogh et al. 2000; van den Bosch et al. 2008; Wetzel et al. 2012), Lu et al. (2014) model the SFR of satellite galaxies using a simple τ model:

$$\dot{M}_{\star, \text{sat}}(t) = \dot{M}_{\star}(t_a) \exp \left(-\frac{t - t_a}{\tau_{\text{sat}}} \right), \quad (5)$$

where t_a is the time when the satellite is accreted into its host and $\dot{M}_{\star}(t_a)$ is the SFR of the satellite galaxy at $t = t_a$. The quantity τ_{sat} is the ‘quenching’ time scale for satellite galaxies, which is modelled as

$$\tau_{\text{sat}} = \tau_{\text{sat},0} \exp \left(-\frac{M_{\star}}{M_{\star,c}} \right), \quad (6)$$

where $\tau_{\text{sat},0}$ is the exponential decay time for a satellite galaxy with a stellar mass of $M_{\star,c}$; both $\tau_{\text{sat},0}$ and $M_{\star,c}$ are treated as free parameters. As discussed in Lu et al. (2014), the choice of τ_{sat} is motivated by the fact that a decreasing quenching time scale with stellar mass seems to be required by the data (Peng et al. 2010; Wetzel et al. 2013), but there is not really a sound physical justification for our adopted form. While the predicted colours and current star formation rates of satellite galaxies depend crucially on the quenching model, the predictions of the SMFs of galaxies that we are interested in here are insensitive to the adopted quenching model.

Each satellite galaxy is assumed to merge with

the central galaxy of its host halo in a time given by the dynamical friction time scale. During the merger, only a fraction f_{TS} of the stellar mass of the satellite is added to the central galaxy; the remainder is considered ‘stripped’ and becomes part of the ‘halo stars’ (Monaco et al. 2006; Conroy et al. 2007). The fraction f_{TS} is treated as a free parameter.

For each galaxy, we track its star formation SFR(t) and mass assembly history $M_{\star}(t)$. At a time step t_i , we obtain the stellar mass following

$$M_{\star}(t_i) = \int_0^{t_i} \text{SFR}(t) R(t_i - t) dt + \sum_a f_{\text{TS}} M_{s,\star}(t_i), \quad (7)$$

which takes into account both the passive evolution and accretion of satellite galaxies denoted by the subscript ‘s’. The summation is over all satellites. $R(t_i - t)$ is the remaining fraction of stellar mass for a stellar population of age $t_i - t$, and is adopted from the stellar evolution model of Bruzual & Charlot (2003) assuming a Chabrier IMF (Chabrier 2003). The total star formation rate is simply the sum of all the progenitors

$$\text{SFR}(t_i) = \text{SFR}_c(t_i) + \sum f_{\text{TS}} \text{SFR}_s(t_i), \quad (8)$$

where the central is denoted by a subscript ‘c’ and satellites by ‘s’.

The luminosity can be calculated in the same way as the stellar mass by replacing $R(t_i - t)$ with the light to mass ratio of a simple stellar population. We use the metallicity - stellar mass relation from Gallazzi et al. (2005). Note that the z - and r -band luminosities are quite insensitive to the assumed metallicity.

2.2 Updating model parameters with recent observational data

In Lu et al. (2014) two sets of observational data were used to constrain the models described above. One is the galaxy SMFs at different redshifts and the other is the z -band cluster galaxy luminosity function from Popesso et al. (2006). The SMFs were those from Baldry et al. (2012) for $z \sim 0$, from Perez-Gonzalez et al. (2008) for $1.0 < z < 1.3$, from Marchesini et al. (2009) for $2.0 < z < 3.0$, and from Stark et al. (2009) for $3.19 < z < 4.73$. The results presented in Lu et al. (2014) are based on Model II constrained by the SMFs alone and Model III constrained by both the SMFs and the cluster galaxy luminosity function. As mentioned above, Model II is unable to match the steep, faint-end upturn observed in the cluster galaxy luminosity function.

As shown in Lu et al. (2014), one way to distinguish Model II and Model III is the difference in their predicted faint-end slope of the SMF at high redshift. The SMF predicted by Model II is quite flat at the low-mass end at all redshifts, while Model III predicts a steepening of the SMF at the low-mass end at high z . More recently, analyses based on deeper surveys provide some evidence for such a steepening.

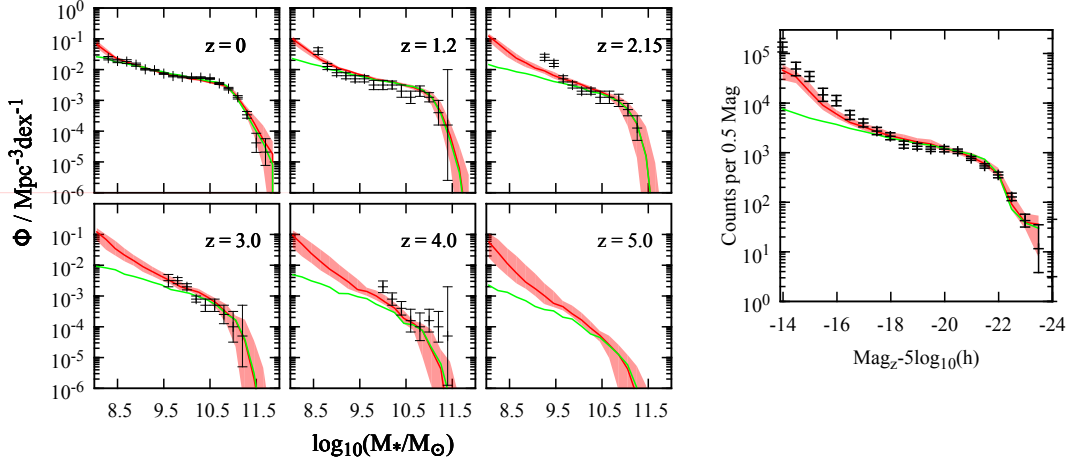


Figure 1. Comparison between the posterior predictions and the constraining data (points with error bars). The high- z SMFs are from Santini et al. (2012). The red curves (best fit) and the bands (95% credible intervals) are predictions of Model III, while the green curves are the predicted means of Model II.

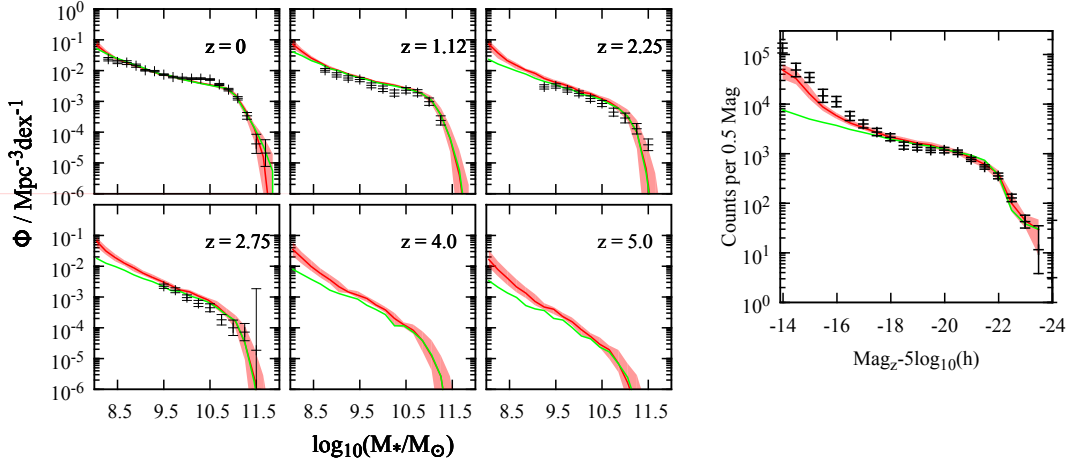


Figure 2. The same as Fig. 1 but the high- z constraining data are from Tomczak et al. (2014).

It is, therefore, interesting to use the new data to update our model parameters. In this paper we use two sets of SMFs recently published. The first is that of Santini et al. (2012) based on the Early Release Science (ERS) data of the Wide Field Camera 3 (WFC3) in the GOODS-S Field, and the SMFs for galaxies in the redshift range between 0.6 and 4.5 are estimated to a stellar mass limit of a few times $10^9 M_\odot$. The second set is that of Tomczak et al. (2014), who estimated the galaxy SMFs in the redshift range 0.2 - 3.0 using data from the FourStar Galaxy Evolution Survey (ZFOURGE) and the Cosmic Assembly Near-IR Deep Extragalactic Legacy Survey (CANDELS). Unfortunately, the two sets are not completely consistent with each other. While at $z < 2.0$ the results obtained by both are similar, at $z > 2$ the SMFs at the low-mass ends obtained by Tomczak et al. (2014) are lower than those obtained by Santini et al. (2012) by a factor of 2. In the present paper we use the two sets of data separately to update our model parameters,

and to check the reliability of our results against uncertainties in the observational data.

In practice, we replace the SMFs at $z > 1$ in Lu et al. (2014) with the new SMFs to constrain the models. As in Lu et al. (2014), we use the MULTINEST method developed by Feroz et al. (2009), which implements the nested sampling algorithm of Skilling (2006), to explore the model parameter space and to make posterior predictions. The new inferences of the model parameters are shown in Table 1 for Model II and in Table 2 for Model III. The comparison between the posterior predictions and the constraining data is shown in Figures 1 and 2. We find that without the cluster data the new data sets alone cannot distinguish decisively between Model II and Model III, because at $z > 3$, the new SMFs are only complete for $M_* > 3 \times 10^9 M_\odot$ where the two models are quite similar. The model inferences based on the Santini et al. (2012) data are similar to those obtained in Lu et al. (2014). The inferences from Tomczak et al. (2014) data are qualitatively the same, except that

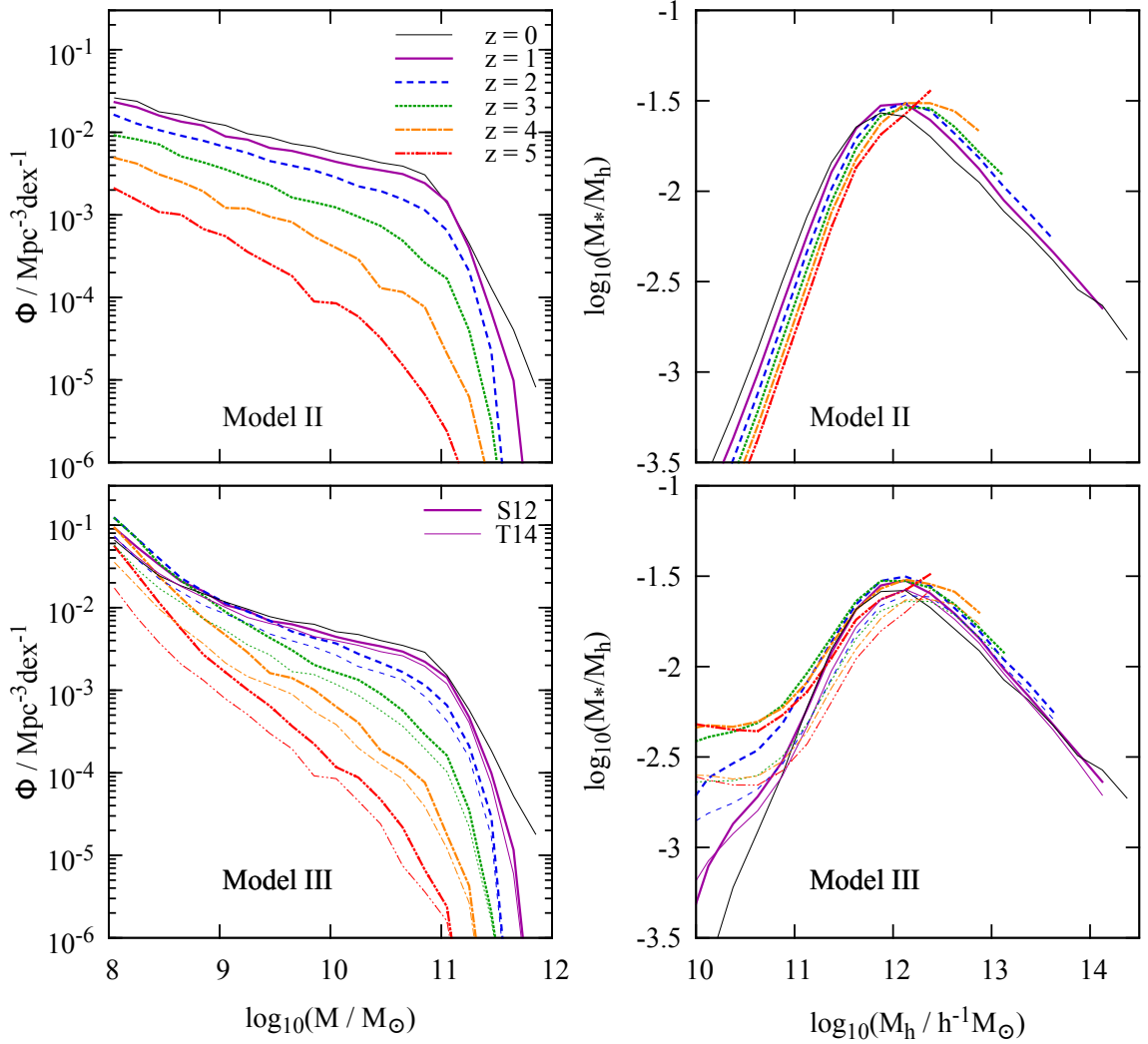


Figure 3. Upper panels: the evolution of the SMF and the M_*/M_h - M_h relation predicted by Model II. Lower panels: predictions of Model III constrained using the SMFs from Santini et al. (2012) (thick lines) and Tomczak et al. (2014) (thin lines).

the inferred star formation rates at $z \geq 3$ in low-mass haloes are lower by a factor of ~ 2 . Note that both models over-predict slightly the SMF in the intermediate redshift range, and even Model III under-predicts the cluster galaxy luminosity function at the faint end somewhat, indicating that either the faint end slope in the cluster galaxy luminosity function is overestimated, or the SMF is under-estimated in the intermediate redshift range, or our Model III is still not flexible enough to match the details of the data.

Figure 3 demonstrates the major differences between Model II and Model III. The upper panels show the SMFs and M_*/M_h at different redshifts predicted by Model II constrained by the $z \approx 0$ SMF of Baldry et al. (2012) together with the SMFs of Santini et al. (2012) at $z > 1$. The thick lines in the lower panels show the predictions of Model III constrained by the

$z \approx 0$ SMF of Baldry et al. (2012), the SMFs of Santini et al. (2012) at $z > 1$, and the cluster galaxy luminosity function of Popesso et al. (2006). As found in Lu et al. (2014), the main difference between Model II and Model III lies in the predicted faint end, especially at high redshift. For comparison, the thin lines in the lower panels show the predictions of Model III but constrained with the SMFs of Tomczak et al. (2014). The model constrained by the Santini et al. (2012) data predicts systematically higher and steeper SMFs at $z \geq 3$ than that constrained by Tomczak et al. (2014). Clearly, accurate observations of the SMFs at $z > 3$ down to a stellar mass limit $M_* < 10^9 M_{\odot}$ are crucial to discriminate the ‘Slow Evolution’ Model II and Model III advocated by Lu et al. (2014). In what follows, we will use the constrained Model II and Model III to make model predictions for a num-

Table 1. The constrained model parameters of Model II, in terms of the means and the variances. The observational constraints used are listed in the first row. B12 is for Baldry et al. (2012), S12 for Santini et al. (2012) and T14 for Tomczak et al. (2014). M_c is in units of $10^{10} h^{-1} M_\odot$, and $M_{*,c}$ is in units of $10^{10} h^{-2} M_\odot$.

	SMF ($z \approx 0$, B12)	SMF ($z \approx 0$, B12)
	SMF ($z \geq 1$, S12)	SMF ($z \geq 1$, T14)
Parameter	mean $\pm\sigma$	mean $\pm\sigma$
α_0	-3.7 ± 0.82	-3.4 ± 0.84
α'	-0.46 ± 0.11	-0.45 ± 0.11
β	3.4 ± 0.86	2.6 ± 0.99
γ	0.89 ± 0.63	1.3 ± 0.77
$\log_{10}(M_c)$	1.7 ± 0.13	1.8 ± 0.18
$\log_{10}(\mathcal{R})$	-1.1 ± 0.34	-1.1 ± 0.45
$\log_{10}(\mathcal{E})$	0.30 ± 0.27	0.017 ± 0.27
$\log_{10}(H_0\tau_{\text{sat},0})$	-0.98 ± 0.17	-0.85 ± 0.13
$\log_{10}(M_{*,c})$	0.81 ± 0.42	0.84 ± 0.38
f_{TS}	0.36 ± 0.17	0.38 ± 0.15

Table 2. The same as Table 1, but for Model III, and the cluster galaxy luminosity function (Popesso et al. 2006) is also used as a constraint.

	SMF ($z \approx 0$, B12)	SMF ($z \approx 0$, B12)
	SMF ($z \geq 1$, S12)	SMF ($z \geq 1$, T14)
Parameter	mean $\pm\sigma$	mean $\pm\sigma$
α_0	-3.0 ± 1.0	-2.7 ± 0.85
α'	-0.36 ± 0.16	-0.37 ± 0.10
β	3.7 ± 0.73	3.9 ± 0.69
γ_a	2.0 ± 0.55	0.58 ± 0.39
γ_b	-0.84 ± 0.14	-0.90 ± 0.08
γ'	-4.4 ± 0.52	-4.2 ± 0.62
z_c	1.8 ± 0.31	2.0 ± 0.38
$\log_{10}(M_c)$	1.6 ± 0.15	1.6 ± 0.13
$\log_{10}(\mathcal{R})$	-0.86 ± 0.18	-0.88 ± 0.17
$\log_{10}(\mathcal{E})$	0.20 ± 0.29	0.07 ± 0.27
$\log_{10}(H_0\tau_{\text{sat},0})$	-0.90 ± 0.16	-0.74 ± 0.04
$\log_{10}(M_{*,c})$	0.34 ± 0.28	0.36 ± 0.17
f_{TS}	0.44 ± 0.22	0.34 ± 0.19
$\log_{10}(e_M)$	0.15 ± 0.04	0.16 ± 0.03

ber of statistical properties of the galaxy population at different redshifts. For clarity, our presentation is based on model parameters constrained by the Santini et al. (2012) SMFs at $z > 1$, i.e. the values listed in the second columns of Tables 1 and 2. We emphasise, however, that none of our results will change qualitatively if the Tomczak et al. (2014) data are used instead to constrain the models.

3 GENERAL TRENDS AND CHARACTERISTIC SCALES

Galaxies can grow their stellar mass either via *in situ* star formation or mergers. In this section, we identify critical halo masses and redshifts to characterise the different stages of stellar mass acquisition as their host haloes grow.

A way to characterise the *in situ* star formation in different haloes at different redshifts is to consider a star formation efficiency which is defined as the ratio between the *in situ* SFR in the central galaxy and the mean halo mass accretion rate $\langle \dot{M}_h(z) \rangle$ multiplied by the universal baryon fraction f_B :

$$\epsilon_{\text{SFR}}(z) \equiv \frac{\text{SFR}(z)}{f_B \langle \dot{M}_h(z) \rangle}. \quad (9)$$

The $\text{SFR}(z)$, defined in Eqs 1 and 2, is implicitly assumed to be an average over galaxies of similar halo mass. For a given halo mass $M_h(t)$, the average mass accretion rate is calculated using

$$\langle \dot{M}_h(t) \rangle \equiv [M_h(t) - \langle M_{\text{prim}}(t - dt) \rangle] / dt, \quad (10)$$

where $\langle M_{\text{prim}} \rangle$ is the average mass of the primary progenitors. The primary progenitors are sampled using the same algorithm adopted to generate the merger trees.

The plots in Figure 4 show ϵ_{SFR} as a function of $M_h(z)$ and z . As one can see, Model II predicts that the *in situ* star formation is most efficient (with $\epsilon_{\text{SFR}} > 0.3$) in a narrow band between $10^{11} h^{-1} M_\odot$ and $10^{12} h^{-1} M_\odot$, with a tilt towards lower mass haloes at lower redshifts. Outside the band, the star formation efficiency drops rapidly towards both higher and lower masses without depending strongly on redshift. This trend of star formation efficiency with halo mass and redshift agrees with the results obtained earlier by Bouche et al. (2010), Behroozi et al. (2013b), Béthermin et al. (2013), Tacchella et al. (2013), and Yang et al. (2013), using different constraints and methods. Model III predicts a similar trend except for haloes with masses $< 10^{11} h^{-1} M_\odot$. Instead of a strong suppression of star formation with decreasing halo mass, the star formation efficiency remains $\sim 1/30$ at $z > 3$ for all $M_h < 10^{11} h^{-1} M_\odot$ haloes.

For central galaxies, another potentially important process that can affect their stellar mass and perhaps the size and morphology is the accretion of satellites. To characterise this process, we calculate the mean galaxy merger rate for haloes of a given mass at a given redshift. We distinguish two different types of mergers: (i) major mergers for which the *stellar mass* ratio between the merging satellite and the central galaxy is $\geq 1/3$ and (ii) minor mergers for which the ratio is between $1/10$ and $1/3$. When calculating the mass ratios, we use the original stellar mass of the satellites before they deposit a fraction $1 - f_{\text{TS}}$ into the stellar halo component. We discuss this choice in the last paragraph of §5. We define the merger rate as the number of mergers per unit time multiplied by the Hubble time $t_H(z) \equiv H(z)^{-1}$. In Figure 4, the red

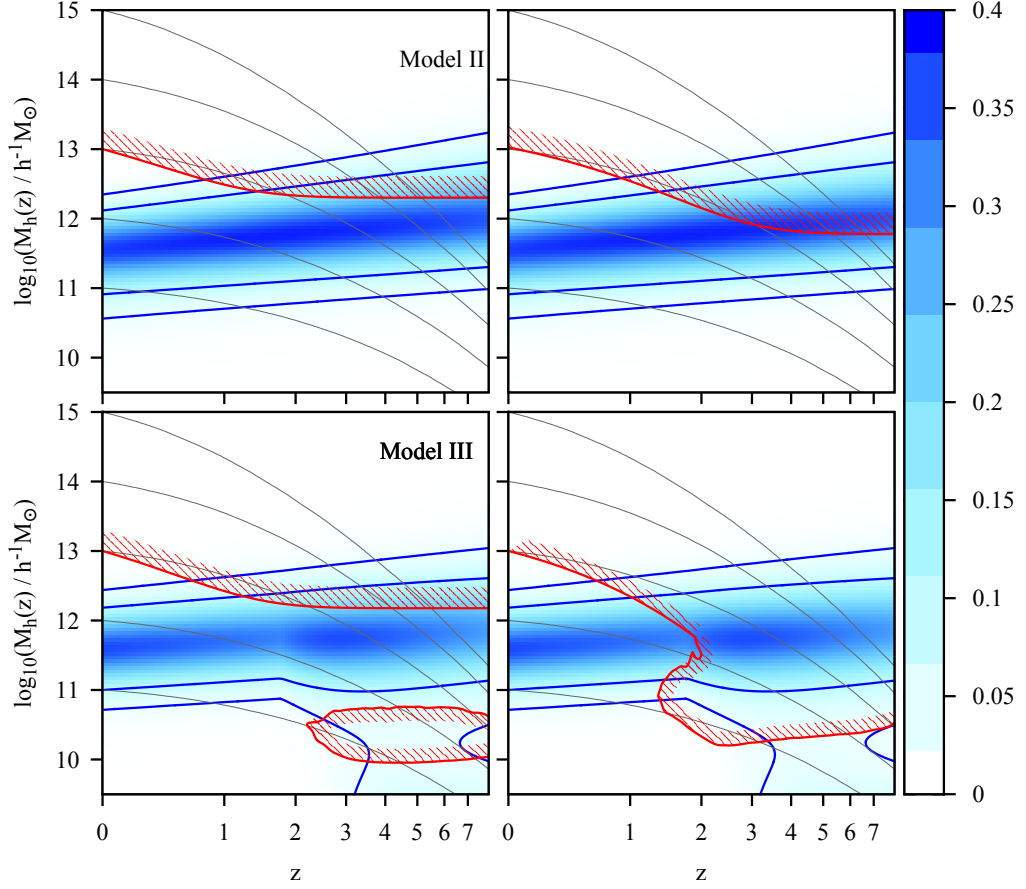


Figure 4. Star formation efficiency and merger rate in the halo mass - redshift plane. The blue shading is the star formation efficiency as indicated in the colour bar on the right. The blue solid lines correspond to star formation efficiency 0.1 (inner two lines) and 0.03 (outer lines). The solid red lines are the loci of one merger event per Hubble time, with the hedged sides corresponding to a higher merger frequency. The left panels are for major mergers (with mass ratios larger than 1/3) and the right panels are for minor mergers with mass ratios between 1/10 and 1/3. The solid grey lines are the mean mass assembly histories of dark matter haloes with present-day masses equal to $10^{11}, 10^{12}, \dots, 10^{15} h^{-1} M_{\odot}$, which are obtained by averaging over the main branches of the merger trees with the same present-day halo mass

. The upper panels are predictions of Model II and the lower panels are the predictions of Model III.

lines are the loci of one merger event per $t_H(z)$ in the halo mass - redshift plane; haloes on the hedged sides of the loci on average have more than one merger per $t_H(z)$. We show results for both major (left panels) and minor (right panels) mergers, and separately for Model II (upper panels) and Model III (lower panels).

For Model II, central galaxies at $z = 0$ have experienced at least one major merger per Hubble time if they are hosted by haloes with masses larger than $\approx 10^{13} h^{-1} M_{\odot}$. At $z > 1$, frequent major mergers only occur for centrals hosted by haloes with masses higher than $\sim 3 \times 10^{12} h^{-1} M_{\odot}$. The predictions of Model III are quite similar for massive haloes, but an additional branch of high major merger rate is also predicted for low mass haloes ($10^{10} h^{-1} M_{\odot} < M_h < 10^{11} h^{-1} M_{\odot}$) at $z > 3$. Comparing the red hedged lines indicating mergers with the star formation efficiency, one can see that most star forming galaxies are not associ-

ated with major mergers, except for central galaxies in low-mass haloes with $M_h = 10^{10} - 10^{11} h^{-1} M_{\odot}$ at $z > 3$, where galaxies can experience major mergers while actively forming stars. Minor mergers are more common. In particular, Model III predicts that active star forming central galaxies in all haloes with $M_h > 10^{10} h^{-1} M_{\odot}$ may have experienced at least one minor merger at $z > 2$.

The following set of functions and scales characterise the star formation efficiency and merger frequency:

- The ridge of the highest star formation efficiency is well described by

$$M_h(z) \approx 3 \times 10^{11} h^{-1} M_{\odot} (1+z)^{0.3}, \quad (11)$$

with a height $\epsilon_{\text{mx}} \sim 0.5$ and a FWHM $\Delta \log_{10}(M_h) \approx 1.0$.

- The line separating frequent from infrequent ma-

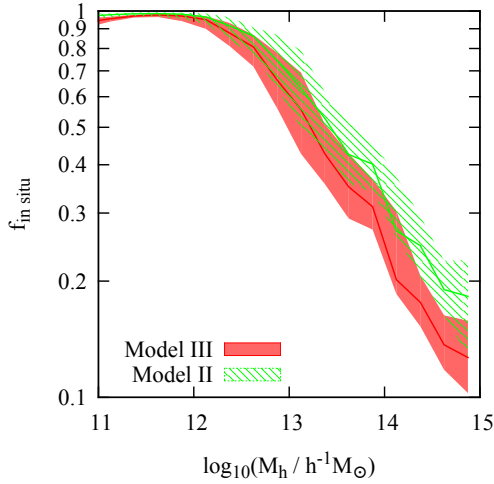


Figure 6. The fraction of stars formed *in situ* in present day central galaxies of haloes with different masses. Shown are the predictions of Model II (green) and Model III (red). The curves are the averages obtained from an ensemble of halo merger trees, while the shaded areas represent the variances among the different halo merger trees.

major mergers for massive haloes can be approximated by

$$M_h(z) \approx 10^{13} h^{-1} M_\odot [0.7 \exp(-z/0.6) + 0.3]. \quad (12)$$

- The line separating frequent from infrequent minor mergers in the entire redshift range for Model II, and at $z < 2$ for Model III, can be approximated by

$$M_h(z) \approx 10^{13} h^{-1} M_\odot [\exp(-z/0.8) + 0.06]. \quad (13)$$

- For Model-III, there is a characteristic redshift, $z_c \sim 2$, above which the star formation efficiency and the major merger frequency are boosted in low mass haloes with $M_h(z) \lesssim 10^{11} h^{-1} M_\odot$, and the minor merger frequency is boosted in all haloes with $M_h(z) > 10^{10} h^{-1} M_\odot$.

4 STAR FORMATION AND STELLAR MASS ASSEMBLY HISTORIES

4.1 Star formation histories

This total SFH (Eq 8), which takes into account the history of the accreted stars and the stars formed *in situ*, is needed when modelling the stellar population of the galaxy. In Figure 5, the black solid lines show the total SFHs of central galaxies in different dark halo mass ranges by averaging over a large number of halo merger histories using the best fit parameters. For comparison, the shaded band in each panel represents the variance among different merger trees of the final halo mass in question. We show results for both Model II (upper panels) and Model-III (lower panels) for five final halo masses, as indicated in each panel.

It is clear that haloes of different present-day masses have different star formation histories. For centrals in massive clusters with $M_h(z = 0) \sim 5 \times$

$10^{14} h^{-1} M_\odot$, the SFR peaks at $z \approx 3$ and the majority of the stars form in a narrow time range, which is about 10 Gyrs ago ($z > 2$). In contrast, for Milky-Way mass haloes, the star formation rate reaches a maximum between $z = 2$ and $z = 1$ and decreases only mildly to the present day. For dwarf galaxies in haloes with $M_h(z = 0) < 10^{11} h^{-1} M_\odot$, the predictions of Model II and Model III are significantly different. For model II, most stars in these dwarf galaxies formed quite late (at $z \leq 1$) and the SFR is roughly a constant over this time interval. In contrast, Model III predicts star formation histories that are bimodal, with an initial star burst at $z > 2$, followed by a constant SFR. As discussed in Lu et al. (2014), although the boost in the star formation rate at high z in low-mass haloes is inferred from the observed upturn in the cluster galaxy luminosity function at the faint end, it also has support from the observed star formation rate function at $z \gtrsim 4$ (Smit et al. 2012), and from the existence of a significant old stellar population in present-day dwarf galaxies (Weisz et al. 2011).

4.2 Stellar mass assembly histories

The average differential assembly histories are shown in Figure 5 as the dashed lines. The assembly history, defined in Eq. (7), takes into account *in situ* star formation, accretion of stars already formed, and mass loss due to stellar evolution. The average differential evolution is obtained by first averaging over the assembly histories of galaxies with the same halo mass, and then taking the time derivative of the mean assembly histories. For both dwarf and Milky-Way sized galaxies, the stellar mass assembly histories are almost parallel to the SFHs except at the beginning of star formation. The difference in amplitude, which is about a factor of 2, owes to the mass loss of evolved stars. This suggests that the assembly of such galaxies is dominated by *in situ* star formation, rather than by the accretion of stars formed in progenitors. We will have a more detailed discussion about this in the following subsection. For massive cluster galaxies, the assembly histories start with a strong episode of *in situ* star formation at $z > 2$, which is followed by a long period of mass accretion at roughly a constant rate.

4.3 In-situ star formation versus accretion

Figure 6 shows the fraction of stars formed *in situ* in present day central galaxies as a function of their host halo mass. The predictions of Model II are plotted as the green line (average) and the green shaded area (with the variance arising from different halo merger trees), while the predictions of Model III are plotted in red. The predictions of the two models are quite similar. For central galaxies in haloes with masses below $10^{12} h^{-1} M_\odot$, almost all the stars are formed *in situ*. This fraction decreases rapidly with increasing halo mass at $M_h > 10^{12} h^{-1} M_\odot$. About 70% of all stars in the central galaxy of a halo with

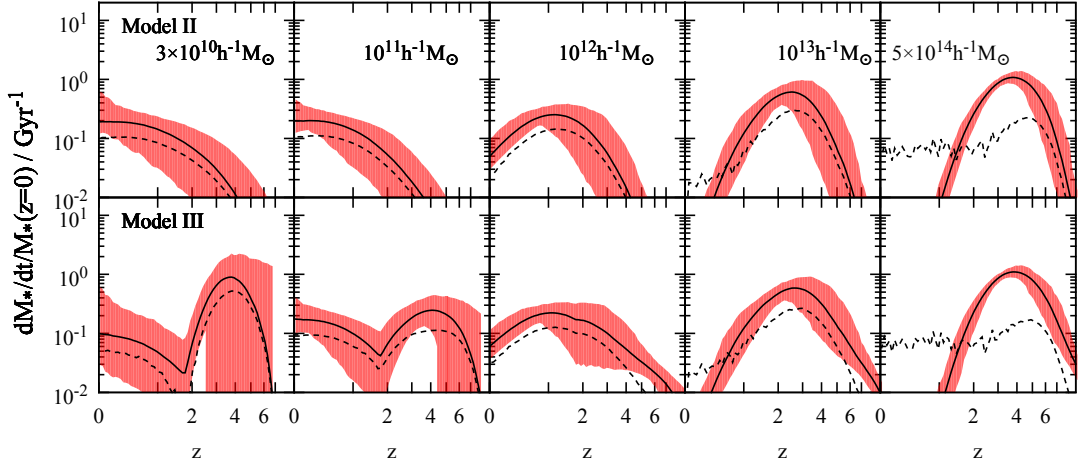


Figure 5. The star formation histories in haloes with different present-day masses (as indicated in the upper panels) predicted by the best-fit parameters of Model II (upper panels) and Model III (lower panels). The thick solid lines are the averages; the shaded areas are the 95% ranges of variance owing to different halo merger histories. The dashed black lines are the average differential assembly histories.

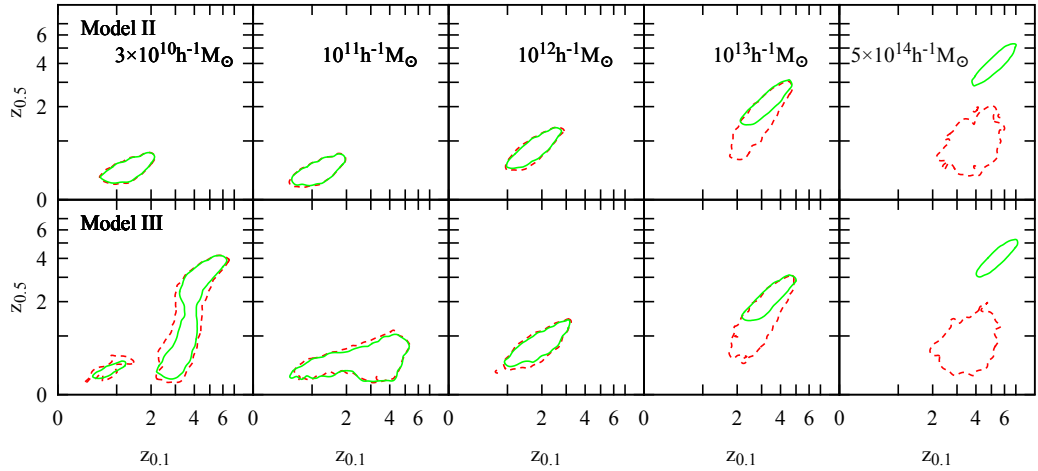


Figure 7. The distribution of the redshift at which 50% ($z_{0.5}$) and 10% ($z_{0.1}$) of the stars in a central galaxy have formed (green solid contours) and have assembled (red dashed contours). The contours are the isodensity lines that enclose 90% of the halo merger trees. We show results for haloes with five masses at $z = 0$, as indicated. The upper panels are the predictions of Model II, while the lower panels are for Model III.

$M_h \sim 10^{13} h^{-1} M_\odot$ are formed *in situ*; for cluster haloes with $M_h \sim 10^{15} h^{-1} M_\odot$ this fraction is about 15%, so about 85% of the stellar mass is acquired through accretion.

4.4 Downsizing versus upsizing

Galaxies of different masses have different star formation (assembly) histories. To characterise these histories in a more quantitative way, we examine the characteristic redshift, z_f , by which a fraction f of the fi-

nal stellar mass in a galaxy has formed (or assembled). Figure 7 shows the distribution of galaxies in the $z_{0.5}$ - $z_{0.1}$ plane for star formation (green contours) and stellar mass assembly (red contours), with the contours delineating the isodensity lines that contain 90% of all the galaxies. The results are again shown for haloes with five different present-day masses, as indicated in the panels, predicted by Model II (the upper 5 panels) and Model III (the lower 5 panels), respectively. For the most massive haloes [$M_h(z=0) > 10^{14} h^{-1} M_\odot$], the star formation time and the assembly time dif-

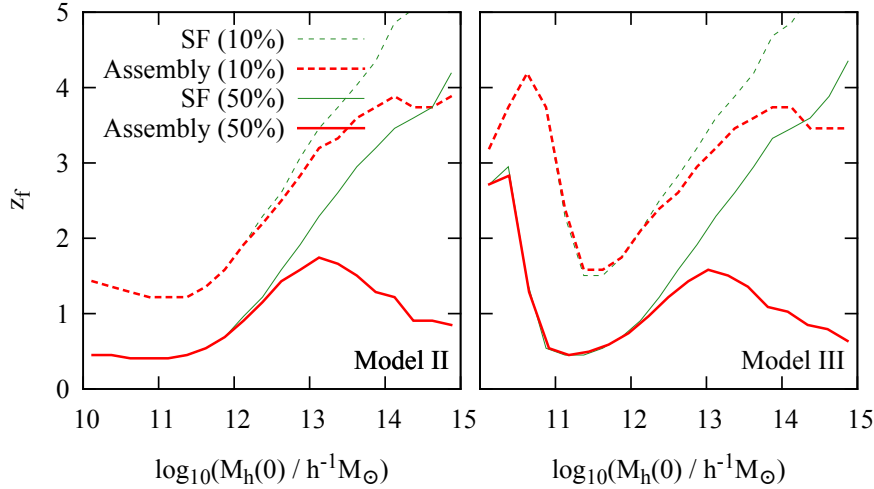


Figure 8. The average characteristic redshifts, $z_{0.5}$ and $z_{0.1}$, as a function of halo mass for star formation (thin lines) and for stellar mass assembly (thick lines).

fer considerably, especially in $z_{0.5}$. On average about 50% of the stellar mass in the central galaxies of such massive haloes form before $z = 4$, but assemble much later at $z \approx 1$. For haloes with masses lower than $10^{13} h^{-1} M_{\odot}$, the star formation time and assembly time are almost identical, indicating that central galaxies in such haloes acquire their stars mostly through *in situ* star formation, as we have already seen in the last subsection. A Milky Way mass galaxy [$M_h(z=0) \sim 10^{12} h^{-1} M_{\odot}$] on average formed about 10% of its stars by $z \approx 2$ and about 50% after $z = 1$. For dwarf galaxies residing in haloes with $M_h(z=0) < 10^{11} h^{-1} M_{\odot}$, Model III predicts diverse formation redshifts. For example, the majority of galaxies residing in $10^{11} h^{-1} M_{\odot}$ haloes are predicted to form 10% of their stars by about $z = 4$, while a fraction is predicted to form their first 10% at much later times: $z \approx 1$. The diversity becomes larger for smaller galaxies: for galaxies in $3 \times 10^{10} h^{-1} M_{\odot}$ haloes, some show star formation as early as that in the centrals of galaxy clusters, while others formed most of their stars after $z \approx 1$. This diversity owes to the transition in the halo accretion histories. Haloes that formed early generally have experienced an early burst phase of star formation, while younger haloes that assembled most of their mass later than the transition redshift did not have such an early star burst.

In Figure 8 we show how the averages of $z_{0.1}$ and $z_{0.5}$ change with halo mass for both star formation (thin lines) and stellar mass assembly (thick lines). For haloes with $M_h(z=0) > 10^{11} h^{-1} M_{\odot}$, both Model II and Model III predict that the centrals of more massive haloes on average form a fixed fraction of their stars earlier, a trend usually referred to as “downsizing” (Fontanot et al. 2009; Weinmann et al. 2012). A similar downsizing trend is also seen in the

stellar mass assembly for haloes with $10^{11} h^{-1} M_{\odot} < M_h(z=0) < 10^{13} h^{-1} M_{\odot}$. However, this trend breaks down in two ways. First, for the most massive haloes [$M_h(z=0) > 10^{13} h^{-1} M_{\odot}$], more massive centrals actually assemble their stars later. At late times, these galaxies tend to build up their mass hierarchically by accreting satellite galaxies, resembling the mass assembly history of the dark matter haloes themselves. Second, although the downsizing trend holds for dwarf galaxies in Model II, the trend predicted by Model III is completely the opposite for these galaxies: on average smaller galaxies tend to be older. This again owes to the boost of star formation in low-mass haloes at high z in Model III.

4.5 The global star formation history

The solid green and red lines in Figure 9 show the star formation rate density (SFRD) predicted by Model II and Model III, respectively. These results take into account star formation in haloes down to a mass of $2 \times 10^9 h^{-1} M_{\odot}$. As shown in Lu et al. (2014), the boost in the SFRD at $z > 3$ of Model III relative to Model II is dominated by star formation in low-mass galaxies hosted by haloes with masses $M_h < 10^{10.5} h^{-1} M_{\odot}$. These galaxies are missed in the current observational data used to derive the SFRD, and so the discrepancy between the prediction of Model III and the observational results at $z > 3$ (shown as error bars in the figure) probably owes to incompleteness in the data. Indeed, if we use the same lower limit of UV magnitude adopted in Bouwens et al. (2012), which is $M_{UV,AB} = -17.7$, to predict the SFRD, we get the results shown by the thin lines, which brings the prediction of Model III into much better agreement with the data. The change in the prediction of Model II is small, because in this model galaxies below the limit

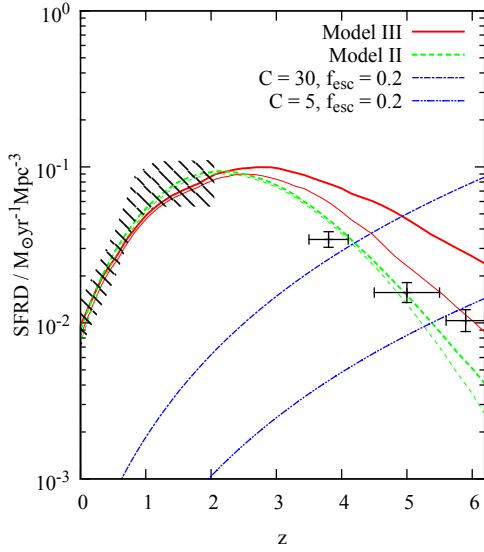


Figure 9. The predicted star formation rate density (solid and dashed lines) and the minimal star formation rate density required to keep the Universe ionised (dot-dashed lines). The hedged band and the data points are from Bouwens et al. (2012). For the model predictions, the solid lines are obtained by integrating down to the merger tree resolution, which is $2 \times 10^9 h^{-1} M_\odot$, and the dashed lines are obtained by integrating down to the detection limit in Bouwens et al. (2012), which is $M_{UV,AB} = -17.7$ or $0.36 M_\odot \text{yr}^{-1}$.

do not make a significant contribution. This demonstrates clearly the importance in observing and modelling very faint galaxies to understand the SFRD at high z .

If one assumes that the Universe is kept ionised by the UV photons from young stars, a minimal SFRD required can be estimated using the equation given by Madau et al. (1999):

$$\frac{\text{SFRD}_{\min}(z)}{M_\odot \text{yr}^{-1} \text{Mpc}^{-3}} \approx 3 \times 10^{-4} \left(\frac{C}{f_{\text{esc}}} \right) \left(\frac{1+z}{6} \right)^3, \quad (14)$$

where C is the clumpiness factor of the IGM and f_{esc} is the average escape fraction of UV photons from star forming galaxies. The normalisation factor is consistent with the Chabrier IMF (Chabrier 2003). The clumpiness factor is expected to evolve with redshift and its value is quite uncertain. Madau et al. (1999) adopted $C = 30$ at $z = 5$ based on the cosmological simulation of Gnedin & Ostriker (1997). More recently, Bolton & Haehnelt (2007) claimed that C at $z = 7$ may be as small as 5. For comparison we show in Figure 9 the minimum SFRD as a function of z assuming $C = 30$ and $C = 5$, with $f_{\text{esc}} = 0.2$ in both cases. If the clumpiness factor is as high as 30, Model III is able to keep the Universe ionised at $z \approx 5$, while SFRD of Model II is too low. However, without better constraints on C and f_{esc} , no stronger statement can be made about the two models.

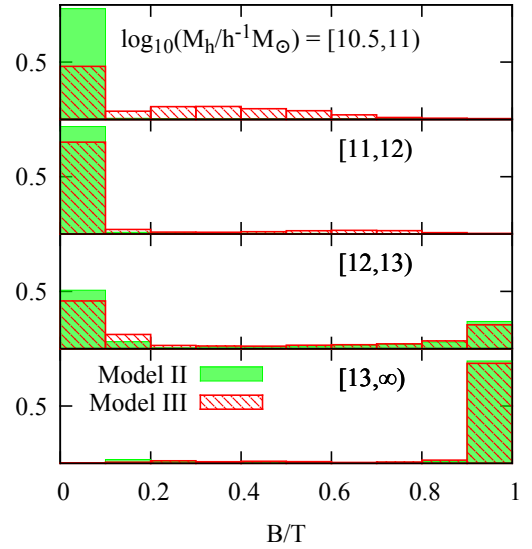


Figure 10. The bulge-to-total mass ratio of local central galaxies as a function of host halo mass. The green histograms are the predictions of Model II while the red hedged histograms are those of Model III.

5 MERGER HISTORY AND THE TRANSFORMATION OF GALAXIES

In this section we characterise the galaxy merger histories in more details and use a simple model to study their implications for the morphological transformation of galaxies.

We make the simple assumption that stellar disks form only through *in situ* star formation, and that a major merger can transform a stellar disk into a spheroid. Here, major mergers are defined in the same way as in §3. The mass of the stellar disk is then simply the total mass of stars formed *in situ* after the last major merger. It should be cautioned, however, that a galactic bulge can be formed in other ways, such as the secular evolution of the disk. The bulge mass defined here, therefore, can only be taken as a lower limit and serves as a simple indicator as to how a central galaxy may be disturbed by infalling satellites. Figure 10 shows the distribution of ‘bulge-to-total’ ratio, B/T , for present-day central galaxies in four halo mass bins.

In cluster haloes, the central galaxies are identified as BCGs in observations. They have been bombarded quite frequently by satellites of different masses. As shown in Figure 11, such galaxies on average have experienced about 5 major mergers and an even larger number of minor mergers during the last period of low *in situ* star formation (defined, quite arbitrarily, as the period after the *in-situ* star formation rate declines to be 1/3 of the peak value). Major mergers contribute about 50% of the total stellar mass. This casts doubt on the scenario in which the late growth and structure of BCGs are assumed to be determined by minor mergers (e.g. Bezanson et al. 2009; van Dokkum et al. 2010; Hilz et al. 2013).

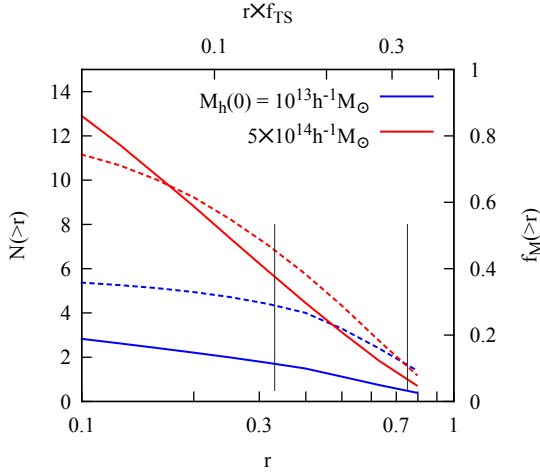


Figure 11. Solid curves: the number of merger events since the *in situ* star formation rate declines to 1/3 of the peak value with a mass ratio $> r$, where r is the stellar mass ratio between the secondary and primary merging progenitors. Dashed curves: the fraction of the total stellar mass acquired by mergers with a mass ratio $> r$. The left vertical line marks $r = 1/3$, which separates major from minor mergers. The results are shown for Model III (the results for Model II are similar for the massive haloes in question). For comparison we also label $r \times f_{TS}$ on the top of the figure, and mark $r \times f_{TS} = 1/3$ by the vertical line on the right. Since f_{TS} is the fraction of the satellite mass that ends up in the central, $r \times f_{TS} = 1/3$ represents that ratio between the satellite mass that actually ends up in the central and the central mass.

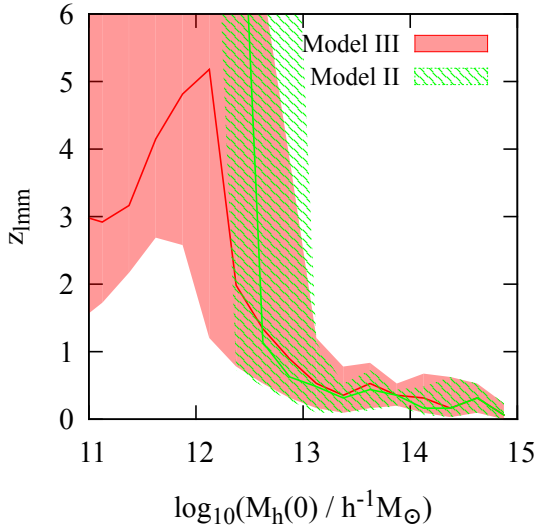


Figure 12. The redshift of the last major merger of present-day central galaxies as a function of host halo mass. The predictions of Model II and Model III are shown in green and red, respectively. Lines are the averages, while the shaded areas enclose the 95% range of variance owing to different merger histories.

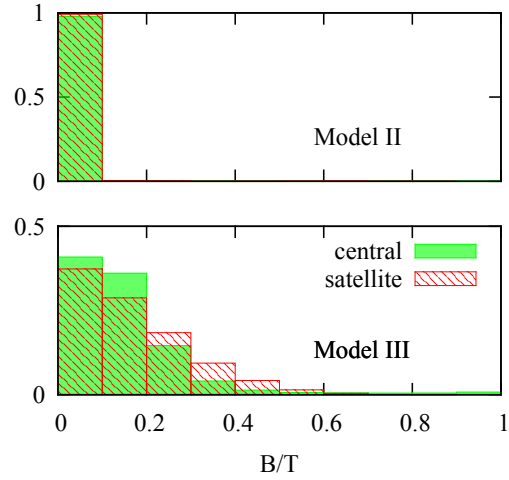


Figure 13. The “bulge” mass fraction of dwarf galaxies with total stellar masses in the range $10^8 h^{-2} M_\odot$ to $10^9 h^{-2} M_\odot$, predicted by Model II (upper panel) and Model III (lower panel) for centrals (green) and for satellites (red).

The last major mergers happened quite recently, at $z \sim 0.5$, as shown in Figure 12. By inspecting images of BCGs at low z , McIntosh et al. (2008) and Tran et al. (2013) did find that a significant fraction of them indeed show signatures of recent major mergers, consistent with our predictions.

For haloes in the mass range $10^{12} h^{-1} M_\odot$ to $10^{13} h^{-1} M_\odot$ there is strong bimodality in their B/T distribution. Significant mergers are sparse in their entire histories: the ‘ellipticals’ in such low mass groups on average only experienced ≈ 1.5 major mergers and no more than 3 mergers with a mass ratio > 0.1 (see Figure 11). The central galaxy is either dominated by bulge, if it has experienced a recent major merger, or remains disk dominated, if such a merger did not occur.

For a Milky Way sized galaxy with $M_h(0) = 10^{11.5} - 10^{12.5} h^{-1} M_\odot$, *in situ* star formation has dominated, while major mergers have been rare since $z \sim 2$. These galaxies, therefore, remain disk dominated, free of any significant major merger - driven bulge components.

The predictions of Model II and Model III differ when it comes to dwarf galaxies. Model II, consistent with many other similar models in the literature, indicates major mergers between dwarf galaxies are extremely rare. Therefore, all the stars are expected to remain in a disk (see the upper panel of Figure 10). In contrast, Model III predicts that most of the galaxies experienced some major mergers during their initial star burst phases ($z > 2$). The exact time when a major merger occurs has large variations for such galaxies, as shown in Figure 12. Major mergers are very rare at $z < 2$ while *in situ* star formation continues, allowing the growth of new disks. The fraction of stars contained in the spheroid depends both on when the last major merger occurs and on the *in situ* star for-

mation that follows. This complexity in star formation history results in diverse morphologies of present day dwarfs, as shown in Figure 10.

Major mergers at early stages of the evolution may shed light on the origin of dwarf ellipticals (dE) and dwarf spheroidal (dSph) galaxies. One popular scenario is galaxy harassment (Moore et al. 1996), in which high speed encounters of a dwarf disk with other galaxies in a dense environment heats up the disk and transform it into a dE or a dSph. However, the predicted kinematics, which shows significant rotation, is at odds with the observational results (e.g. Geha et al. 2003; Toloba et al. 2013). Our result here suggests that some of the slow rotators could be the remnants of early major mergers between dwarf galaxies. The lower panel of Figure 13 shows B/T of both dwarf centrals and satellites predicted by Model III, with the latter skewed towards higher B/T . In contrast, Model II indicates that all dwarf galaxies are strongly disk dominated. However, the predicted fraction of bulge-dominated dwarfs by Model III may be too low to account for the total population of dE's and dSph's. It is likely that later evolution, such as harassment, also plays a role in transforming the disk component, making the bulge components more dominant.

It should be pointed out that the above discussion is based on the value of r , namely the ratio between the original secondary mass and the primary mass. As shown above, our model predicts that only a fraction, $f_{TS} \sim 0.4$, of the original mass of the secondary is added to the central after a merger while the rest is stripped and deposited as halo stars. If the stripping occurred at large distances from the central, the secondary mass at the time of merger would be $r \times f_{TS}$. For comparison, the values of this quantity are labelled on the top of Figure 11. As is clear, in this case major mergers, still defined by a mass ratio $\geq 1/3$, would be rare for all galaxies. However, this scenario may not be realistic. Observations show that halo stars are mostly identified around central galaxies and, as we will see below, the amount of halo stars predicted by our models is consistent with observations (Bernardi et al. 2013). This suggests that stripping of stars most likely occurs when the secondary is close to the primary, and so the mass ratio, r , defined above is more relevant when considering the mutual gravitational interaction between the merging galaxies.

6 STELLAR POPULATIONS

6.1 Stellar ages

Observationally, the star formation histories (SFHs) of individual galaxies can be estimated from their stellar populations. One popular way to do this is to use the spectra of galaxies, which contain information about the SFH, initial mass function (IMF), chemical enrichment history and dust content of galaxies. In Figure 14, we compare the average stellar ages predicted by Model II and Model III with the observational results of SDSS galaxies obtained by Gallazzi et al.

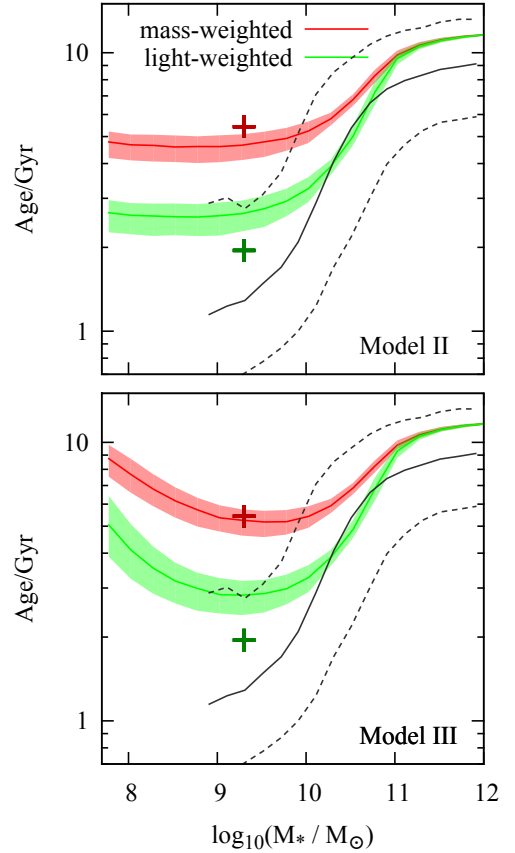


Figure 14. The stellar age as a function of stellar mass predicted by Model II (upper panel) and Model III (lower panel). Both mass-weighted and light (luminosity)-weighted averages are shown, with the bands representing the 95% percentile of halo merger histories. The lines show the light-weighted averages of stellar ages obtained by Gallazzi et al. (2005) from the SDSS, with the solid line being the median and the two dashed lines representing the 16% and 84% percentile. The crosses are the mass-weighted (dark red) and light-weighted (green) ages of the LMC obtained from the star formation history given by Weisz et al. (2013).

(2005). The observational stellar ages are determined by simultaneously fitting five spectral absorption features that break some degeneracies in spectral synthesis parameters. The weighted age of a galaxy is defined as

$$\text{Age} = \frac{\int_0^\infty \text{SFR}(t)f(t)t dt}{\int_0^\infty \text{SFR}(t)f(t) dt}, \quad (15)$$

where $f(t)$ is either the fraction of the remaining stellar mass or the luminosity of a simple stellar population with age t . In Figure 14 we plot the average ages weighted either by stellar mass (red bands) or by the r -band luminosity (green bands). The observational ages, with the median shown by the solid line and the 16 and 84 percentile by the dashed lines, are also weighted by the r -band luminosity, so a direct

comparison between the model and the data can be made. The SDSS galaxies cover a stellar mass range between 10^9 and $10^{12} M_{\odot}$, where the observed age increases with stellar mass generally, and increases sharply around $10^{10} M_{\odot}$. The model predictions agree with the observational data only qualitatively: the predicted ages are systematically older than that observed between $10^9 M_{\odot}$ and $10^{10} M_{\odot}$. Similar discrepancies have also been found by Lu Y. et al. (2013) using semi-analytic models.

This discrepancy may indicate an intrinsic deficiency in the approach adopted here or in similar approaches in the literature. By matching only SMFs of galaxies, our model may be insensitive to the star formation history in the recent past. For example, an enhancement in recent star formation may contribute little to the total stellar mass, and so is not well captured in our model, but can significantly increase the optical luminosity, thereby decreasing the light-weighted age. As a demonstration, the upper cross in Figure 14 shows the stellar mass weighted age of stars in the LMC based on the star formation history derived from the colour magnitude diagram of resolved stars (Weisz et al. 2013). Our model predictions match the observation well. For comparison, the lower cross shows the r -band luminosity-weighted age obtained from the same star formation history with our adopted spectral synthesis model. The age so obtained lies below the green band, because our average model underpredicts the current star formation rate of the LMC.

There are uncertainties in the observational data too. It is in general difficult to distinguish stars that formed about 8-10 Gyrs ago from those that formed 4-5 Gyrs ago from an analysis of the optical-NIR spectra (e.g. Bruzual & Charlot 2003; Pacifici et al. 2012). Basically the UV light provides information about recent star formation, while strong Balmer absorption lines are sensitive only to intermediate-age (1-3 Gyrs old) stars, but one cannot distinguish stars older than 4 Gyrs. Thus, it is possible that the average stellar ages derived from the observational data have missed the contribution of such an old population.

6.2 Halo Stars

In our simple prescription for galaxy mergers, a constant fraction f_{TS} of the original stellar mass of the merging satellite is accreted by the central, and the rest is deposited in a diffuse component, referred to as intracluster stars in clusters or as halo stars in general. f_{TS} is constrained to be about 40%, although the uncertainty is quite large (Tables 1 and 2). This low value of f_{TS} is driven predominantly by the observed SMFs at the massive end, i.e. with $M_{\star} \gtrsim 10^{11} M_{\odot}$ corresponding to $M_h > 10^{13} h^{-1} M_{\odot}$. Had we set $f_{TS} = 1$, i.e. if all the original mass in an accreted satellite were added to the central, we would get a SMF that is significantly higher than the observations of Baldry et al. (2012) at the very massive end (thick black line in Figure 15).

Recent analyses show that the most massive

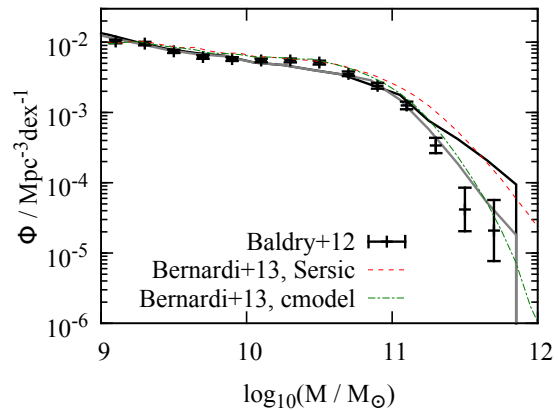


Figure 15. The stellar mass function of galaxies predicted by Model III (grey line) compared to the prediction of the same model but assuming no stripping of satellites, i.e. $f_{TS} = 1$ (the thick black line). The data points are the observational data of Baldry et al. (2012). The green dot-dashed line is the SMF obtained by Bernardi et al. (2013) using SDSS ‘cmodel’ magnitudes, while the red dashed line is the result obtained by the same authors using the magnitudes within the entire Sersic profiles (i.e. integrated to infinity) obtained by Simard et al. (2011).

galaxies (with $M_{\star} > 10^{11} M_{\odot}$) tend to have extended wings in their light profiles. This makes the luminosity (stellar mass) measurements of these galaxies quite uncertain. As shown by Bernardi et al. (2013) and He et al. (2013), using different methods and light profiles to fit galaxy images can lead to a factor of 2 difference in the estimated luminosity of a massive galaxy. The effect on the derived SMF can be seen in Figure 15 comparing the red dashed line with the green dot-dashed line. It is interesting to note that our model prediction assuming $f_{TS} = 1$ is consistent with the SMF obtained by Bernardi et al. (2013) using the magnitudes within the entire Sersic profiles (the red line) obtained by Simard et al. (2011). This suggests that the halo component defined in our model may simply be the extended profiles of massive galaxies that are missing in the SMFs we use as constraints.

Figure 16 shows the ratio between the total mass of halo stars and the stellar mass of the central galaxy as a function of host halo mass. In a cluster as massive as $10^{15} h^{-1} M_{\odot}$, the mass in the diffuse component is about 2 - 3 times as high as that of the central galaxy and in a group sized halo of mass $\sim 10^{13} h^{-1} M_{\odot}$, the ratio is about 1. It drops rapidly towards lower halo mass. In a Milky Way mass halo, the predicted ratio is only a few percent. The flattening at the even lower mass end predicted by Model III owes to the boosted star formation at high z in low-mass haloes. The results for low-mass haloes should be taken with caution. As mentioned above, our model assumes a constant f_{TS} and it is constrained primarily by the SMFs at the massive end. It is unclear whether the same number also applies to galaxies with lower masses.

To understand the stellar population of the halo

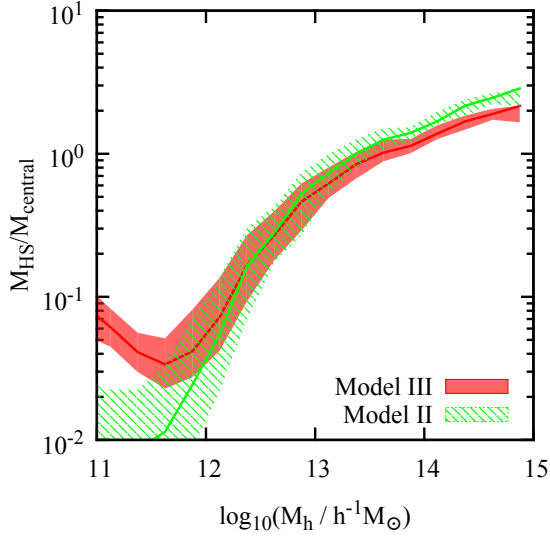


Figure 16. The mass ratio between halo stars and the stellar mass of the central galaxy as a function of host halo mass at $z = 0$. The green band is the prediction of Model II and the red band that of Model III. Here again the widths of the bands represent the variance among different halo merger trees.

stars, we make a census of their formation time and location, in terms of redshift and the stellar mass of the host galaxy in which they formed, respectively. We show the result as the solid contours in Figure 17. For comparison, we also plot the results for stars in the central galaxies as the dashed contours. The stellar mass can be taken as crude proxy to stellar metallicity as the two are found to be correlated for local galaxies (Gallazzi et al. 2005). The stellar metallicity increases with stellar mass for galaxies with stellar masses below $2 \times 10^{10} M_\odot$ and becomes saturated at about solar metallicity above this mass (indicated by the horizontal lines in Figure 17).

Compared to the stars in the central galaxy, the halo stars in a Milky Way sized halo form a distinct population: the mass weighted age of the halo stars is roughly about 9-10 Gyr, in contrast with the central galaxy, which is about 6 Gyr. These halo stars formed in progenitors with mass lower than the horizontal line, suggesting a metallicity much lower than the solar value. This is qualitatively consistent with the recent observations of M31 (Bernard et al. 2014). In massive clusters, on the other hand, the stellar populations in both the central galaxy and the halo component are quite homogeneous, with ages of ~ 10 Gyr and with nearly solar metallicity. This prediction can be checked by studying the stellar age and metallicity of halo stars in clusters.

7 SUMMARY AND DISCUSSION

In a previous paper (Lu et al. 2014), we developed an empirical model to describe the star formation

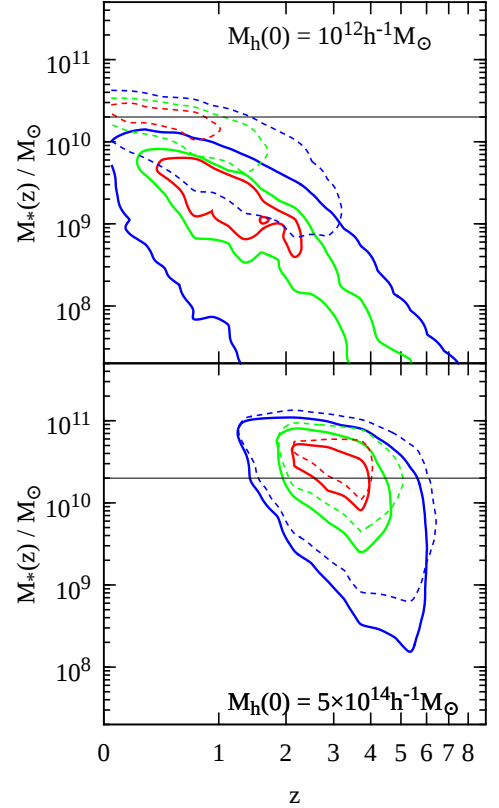


Figure 17. The solid contours show the formation redshift and location (i.e. the stellar mass of the galaxy) of the halo stars. Red, green and blue contours enclose 30%, 60% and 90% of the stars, respectively. The dashed contours are the same as the solid ones but for stars in central galaxies. We only show Model III (Model II is similar). Results are shown for Milky Way mass haloes (upper panel) and massive cluster haloes (lower panel). The horizontal lines mark $M_* = 2 \times 10^{10} M_\odot$, above which the stellar metallicity begin to saturate (Gallazzi et al. 2005).

rates of central galaxies in haloes of different masses at different redshifts. A series of nested models were constructed to accommodate more and more observational constraints. We found that Model II, which represents a class of ‘Slow Evolution’ models in the literature, can reproduce the SMFs since $z = 4$, but fails to accommodate the cluster galaxy luminosity function, the steep SFR-functions at high z , and the old stellar population seen in local dwarf galaxies. We also found that Model III is the simplest model family that can match all these observational data well. In the present paper, we use the same models, but with model parameters updated using recent observational data of the galaxy SMFs at high z . The results presented here confirm and re-enforce those of Lu et al. (2014). In particular, the constrained Model III predicts much steeper SMFs at $z \geq 4$ than Model II. Since the publication of Lu et al. (2014), two addi-

tional studies have presented evidence in support of this picture (Madau et al. 2014; Weisz et al. 2014). These results suggest that the class of ‘Slow Evolution’ models in the literature (Yang et al. 2013; Behroozi et al. 2013a; Béthermin et al. 2013), in which star formation in haloes with $M_h < 10^{11} h^{-1} M_\odot$ are suppressed at high z , are insufficient to describe the evolution of the galaxy population.

We use our constrained model parameters to characterise the star formation and stellar mass assembly histories as well as the merger histories of galaxies of different masses. The results are summarised in the following.

First, the evolution of the galaxy population is found to be characterised by a number of characteristic halo mass scales:

(i) A mass scale of $10^{13} h^{-1} M_\odot$ at $z = 0$, decreasing to $\sim 3 \times 10^{12} h^{-1} M_\odot$ at $z > 2$, above which *in situ* star formation drops rapidly, and the central galaxies experience frequent major mergers most of which will be dry.

(ii) A mass scale of $3 \times 10^{11} h^{-1} M_\odot$ at $z = 0$, increasing to $10^{12} h^{-1} M_\odot$ at high z , at which the efficiency of *in situ* star formation reaches a maximum, with a SFR as high as about half of the baryon accretion rate into the host halo. Major mergers are rare in this halo mass range.

(iii) A mass scale of $10^{11} h^{-1} M_\odot$ at $z > 3$, below which *in situ* star formation has a rate about 0.1 times the baryon accretion rate into the host halo. On average, one or two major mergers are expected to occur for the central galaxies.

Second, galaxies hosted by haloes of different masses follow distinct star formation and assembly histories. Based on the characteristic halo masses given above, central galaxies can be divided roughly into three different categories according to their formation and assembly histories:

(i) For haloes with $M_h > 10^{13} h^{-1} M_\odot$, a strong *in situ* star formation rate declines rapidly after reaching its peak value, and is followed by significant accretion of stars from satellites. For such massive systems, more massive galaxies tend to assemble their stellar mass later, contrary to the downsizing trends observed for lower mass galaxies.

(ii) For haloes with masses $10^{11} h^{-1} M_\odot < M_h < 10^{13} h^{-1} M_\odot$, mass assembly by accretion of satellites is not important, and the star formation is delayed relative to the formation of the host halo.

(iii) For haloes with masses below $10^{11} h^{-1} M_\odot$, assembly by accretion is again unimportant. The star formation history is characterised by a burst at $z > 2$ and a nearly constant star formation rate after $z = 1$. The relative importance of the early star formation increases with decreasing halo mass, and the ‘downsizing’ trend is reversed.

Third, we use the merger history of the model galaxies to predict the bulge to total mass ratios of present galaxies. The average bulge mass fraction is found to depend strongly on halo mass:

(i) In cluster sized haloes with $M_h > 3 \times 10^{13} h^{-1} M_\odot$, almost all the centrals are ellipticals formed through frequent major mergers.

(ii) In group sized haloes with masses between $3 \times 10^{12} h^{-1} M_\odot$ and $3 \times 10^{13} h^{-1} M_\odot$, the distribution of the bulge-to-total ratio of the central galaxies is strongly bimodal. Those galaxies that experienced a recent major merger are spheroid dominated, whereas the others are free of any significant merger-driven bulge.

(iii) For haloes with masses $3 \times 10^{11} h^{-1} M_\odot < M_h < 3 \times 10^{12} h^{-1} M_\odot$, central galaxies with a significant merger-driven bulge are extremely rare.

(iv) For dwarf galaxies, half of them have significant (with $B/T > 10\%$) spheroidal components formed during their early star burst phase ($z > z_c \approx 2$). Satellite galaxies of similar masses tend to have a larger bulge fraction than centrals.

We emphasise again that bulges can form in various other ways than through major mergers, and that our prediction only applies to major merger-driven bulges.

Finally, we have made predictions for the amount of halo stars, and when and where these stars form in comparison with stars in the corresponding central galaxies. The results are:

(i) In a Milky Way mass halo, the total mass in halo stars is 2 to 5 percent of the mass of the central galaxy, and this number increases to $\sim 100\%$ in haloes with $M_h \sim 10^{13} h^{-1} M_\odot$, and to about 200% to 300% in massive clusters.

(ii) In a Milky Way mass halo, the stars in the central galaxy and halo stars form two distinct stellar populations, with the latter being older and poorer in metals. In contrast, these two components form a quite homogeneous population (old and with solar metallicity) in massive clusters.

All these results are obtained in an empirical way, independent of any detailed assumptions about the underlying physical processes that drive the evolution of the galaxy population. Clearly, our results should be compared with the predictions of numerical simulations and/or semi-analytical models to constrain theories of galaxy formation. We will come back to this in a forthcoming paper.

ACKNOWLEDGEMENTS

We thank Stephane Charlot for discussion, and Ryan Quadri for providing the ZFOURGE/CANDELS stellar mass functions. We would like to acknowledge the support of NSF AST-1109354 and NSF AST-0908334.

REFERENCES

- Avila-Reese V., Firmani C., 2011, RMxAC, 40, 27
- Baldry I.K. et al. 2012, MNRAS, 421, 621
- Balogh M.L., Navarro J.F., Morris S.L., 2000, ApJ, 540, 113

- Behroozi P.S., Conroy C., Wechsler R.H., 2010, *ApJ*, 717, 379
- Behroozi P.S., Wechsler R.H., Conroy C., 2013, *ApJ*, 762, 31
- Behroozi P.S., Wechsler R.H., Conroy C., 2013, *ApJ*, 770, 57
- Bernard E. et al., 2014, arXiv:1406.2247
- Bernardi et al., 2013, arXiv:1304.7778
- B  thermin M., et al. 2013, preprint, arXiv:1304.3936
- Bezanson Rachel, van Dokkum Pieter G., Tal Tomer, Marchesini Danilo, Kriek Mariska, Franx Marijn & Coppi, Paolo, 2009, *ApJ*, 697, 1290
- Bolton J. S. & Haehnelt M. G., 2007, *MNRAS*, 382, 325
- Bouche et al., 2010, *ApJ*, 718, 1001
- Bouwens R.J. et al., 2012, *ApJ*, 754, 83
- Bruzual G. & Charlot S., 2003, *MNRAS*, 344, 1000
- Chabrier G., 2003, *PASP*, 115, 763
- Cole S., Helly J., Frenk C. S., Parkinson H., 2008, *MNRAS*, 383, 546
- Conroy C., Wechsler R.H. & Kravtsov A.V., 2007, *ApJ*, 668, 826
- Conroy C. & Wechsler R.H., 2009, *ApJ*, 696, 620
- Fontanot F., De Lucia G., Monaco P., Somerville R. & Santini P., 2009, *MNRAS*, 397, 1776
- Feroz F., Hobson M.P. & Bridges, M., 2009, *MNRAS*, 398, 1601
- Gallazzi A., Charlot S., Brinchmann J., White S.D.M. & Tremonti C.A., 2005, *MNRAS*, 362, 41
- Geha M., Guhathakurta P. & van der Marel R. P., 2003, *AJ*, 126, 1794
- Gnedin N.Y., Ostriker J.P., 1997, *ApJ*, 486, 581
- He Y. Q., Xia X. Y., Hao C. N., Jing Y. P., Mao S., Li C., 2013, *ApJ*, 773, 37
- Hilz M., Naab T. & Ostriker J. P., 2013, *MNRAS*, 429, 2924
- Jiang F., van den Bosch F.C., 2014, *MNRAS*, in press (arXiv:1311.5225)
- Kauffmann G., White S.D.M., Guiderdoni B., 1993, *MNRAS*, 264, 201
- Komatsu et al., 2011, *ApJS*, 192, 18
- Leauthaud A., et al., 2012a, *ApJ*, 744, 159
- Leauthaud A., et al., 2012b, *ApJ*, 746, 95
- Leitner S.N., 2012, *ApJ*, 745, 149
- Lu Y. et al., 2013, arXiv:1312.3233
- Lu Z., Mo, H. J., Lu Y., Katz N., Weinberg M.D., van den Bosch F.C., Yang X., 2014, *MNRAS*, 439, 1294
- Madau P., Haardt F., Rees M. J., 1999, *ApJ*, 514, 648
- Madau Piero, Weisz Daniel R. & Conroy Charlie, 2014, arXiv:1406.0838
- Marchesini D., van Dokkum P.G., Frster Schreiber N.M., Franx M., Labb I., Wuyts S., 2009, *ApJ*, 701, 1765
- McIntosh et al., 2008, *MNRAS*, 388, 1537
- Monaco P., Murante G., Borgani S. & Fontanot F., 2006, *ApJ*, 652, 89
- Moore B., Katz N., Lake G., Dressler A., Oemler A., 1996, *Nature*, 379, 613
- Moster B.P., Somerville R.S. Maulbetsch C., van den Bosch F.C., Maccio A.V., Naab T., Oser L., 2010, *ApJ*, 710, 903
- Moster B.P., Naab T., White S.D.M., 2013, *MNRAS*, 428, 3121
- Pacifici C., Charlot S., Blaizot J. & Brinchmann J., 2012, *MNRAS*, 421, 2002
- Parkinson H., Cole S. & Helly J., 2008, *MNRAS*, 383, 557
- Peng Y-j., et al. 2010, *ApJ*, 721, 193
- Perez-Gonzalez P.G., et al., 2008, *ApJ*, 675, 234
- Popesso P., Biviano A., Bhlinger H. & Romaniello M., 2006, *A&A*, 445, 29
- Santini et al., 2012, *AA*, 538, 33
- Skilling J., 2006, *Bayesian Analysis*, 1, 833
- Simard L., Mendel J. T., Patton D. R., Ellison S. L., McConnachie A. W., 2011, *ApJS*, 196, 11
- Smit R., Bouwens R.J., Franx M., Illingworth G.D., Labbe I., Oesch P.A. & van Dokkum P.G., 2012, *ApJ*, 756, 14S
- Stark D.P., Ellis R.S., Bunker A., Bundy K., Targett T., Benson A. & Lacy M., 2009, *ApJ*, 697, 1493S
- Tacchella S., Trenti M. & Carollo M., 2013, *ApJ*, 768, 37
- Toloba E., Boselli A., Peletier R. F., Falcon-Barroso J., van de Ven G., Gorgas J., 2013, *A&A*, 557, 2
- Tomczak A. R., et al. 2014, *ApJ*, accepted for publication, arXiv:1309.5972
- Tran Kim-Vy, J. Brough S., Gebhardt K., von der Linden A., Couch W.J., Sharp R., 2013, eprint arXiv:1310.7587
- van den Bosch F.C., 1998, *ApJ*, 507, 601
- van den Bosch F.C., 2002, *MNRAS*, 331, 98
- van den Bosch F.C., Norberg P., Mo H.J., Yang X., 2004, *MNRAS*, 352, 1302
- van den Bosch F.C., Aquino D., Yang X., Mo H.J., Pasquali A., McIntosh D.H., Weinmann S.M., Kang X., 2008, *MNRAS*, 387, 79
- van Dokkum et al., 2010, *ApJ*, 709, 1018
- Wang L., et al., 2013, *MNRAS*, 431, 648
- Weinmann S. et al., 2012, *MNRAS*, 426, 2797
- Weisz D.R., et al., 2011, *ApJ*, 739, 5
- Weisz D.R., et al., 2013, *MNRAS*, 431, 364
- Weisz D. R. et al., 2014, arXiv:1404.7144
- Wetzel A.R., Tinker J.L., Conroy C., 2012, *MNRAS*, 424, 232
- Wetzel A.R., Tinker J.L., Conroy C. & van den Bosch F.C., 2013, *MNRAS*, 432, 336
- Yang X., Mo H.J., van den Bosch F., 2009, *ApJ*, 693, 830
- Yang X., Mo H.J., van den Bosch F.C., Zhang Y., Han J., 2012, *ApJ*, 752, 41
- Yang X., Mo H.J., van den Bosch F.C., Bonaca A., Li S., Lu Y., Lu Y., Lu Z., 2013, *ApJ*, 770, 115